Optical probe into the doping modulation of the magnetic Weyl semimetal $Co_3Sn_2S_2$

L. Wang,[1,*] S. Zhang,[2,*] B. B. Wang,[2] B. X. Gao,[1] L. Y. Cao,[1] X. T. Zhang,[1] X. Y. Zhang,[1] E. K. Liu,[2,†] and R. Y. Chen[1,‡]

[1]*Center for Advanced Quantum Studies and Department of Physics, Beijing Normal University, Beijing 100875, China*

[2]*State Key Laboratory for Magnetism, Institute of Physics, Chinese Academy of Sciences, Beijing 100190, China*

(Received 28 December 2023; revised 29 May 2024; accepted 26 June 2024; published 15 July 2024)

The magnetic Weyl semimetal $Co_3Sn_2S_2$ is extensively investigated due to its giant anomalous Hall effect (AHE). Recent studies demonstrate that the AHE can be effectively tuned by multielectron Ni doping. To reveal the underlying mechanism of this significant manipulation, it is crucial to explore the band-structure modification caused by Ni doping. Here, we study the electrodynamics of both pristine and Ni-doped $Co_{3-x}Ni_xSn_2S_2$ with $x = 0$, 0.11, and 0.17 by infrared spectroscopy. We find that the inverted energy gap around the Fermi level (E_F) gets smaller at $x = 0.11$, which is supposed to enhance the Berry curvature and therefore increases the AHE. Then E_F moves out of this gap at $x = 0.17$. We also observe the evidence of band broadening caused by doping. Our results provide detailed information about the band structure of $Co_{3-x}Ni_xSn_2S_2$ at different doping levels, which will help to guide further studies on the chemical tuning of AHE.

DOI: 10.1103/PhysRevB.110.035141

I. INTRODUCTION

The anomalous Hall effect (AHE) was initially discovered in ferromagnetic (FM) materials with a magnitude proportional to the magnetization [1,2]. For a very long time, AHE was considered as a unique property of time-symmetry-breaking systems with a net magnetization, whose origination seemed too complicated to be clearly revealed. In the 1980's, the development of the Berry phase theory has brought a breakthrough in understanding the physical mechanism of AHE [3], which substantially advanced our perspectives of this phenomenon. Nowadays, it is generally believed that AHE can be generated from two different mechanisms: the extrinsic mechanism caused by the scattering effect (skew scattering [4] and side jump [5]) and the intrinsic mechanism related to Berry curvature [6,7]. Among them, the intrinsic contribution is directly related to the topological properties of the Bloch state. Therefore, the anomalous Hall conductivity (AHC) depends only on the band structure of the ideal crystal lattice, which can be calculated directly by the Kubo formula [7–9].

A great number of materials have been reported to cast giant intrinsic AHE, such as the kagome metal Nd_3Al [10], Weyl semimetal Mn_3Sn [11], Dirac semimetal Fe_3Sn_2 [12], topological insulator $MnBi_2Te_4$ [13], etc. Among them, Weyl semimetals are of special interest as the Berry curvature near the Weyl points is inherently divergent, which is supposed to contribute a large AHC when they are near the Fermi surface [14–16]. Moreover, the AHC generated by the topologically protected Weyl point is rather robust to perturbations such as lattice distortion and chemical substitution [14,17], which is a vital advantage for developing next-generation spintronic devices.

$Co_3Sn_2S_2$ is a typical magnetic Weyl semimetal with an AHC up to $\sim$1130 $\Omega^{-1}\,cm^{-1}$ and an anomalous Hall angle of $\sim$20%. Previous studies have shown that its large AHE is dominated by the divergent Berry curvature near the Weyl point at $\sim$60 meV above the Fermi level (E_F) [18,19]. Subsequently, attempts were made to modulate the AHC of the material by doping holes or electrons in order to fine-tune the relative position of the E_F and the Weyl point [20–24]. Thereinto, Shen *et al.* have succeeded in elevating the AHC of $Co_3Sn_2S_2$ by multielectron Ni doping, which reaches a maximum in $Co_{3-x}Ni_xSn_2S_2$ when $x = 0.11$ ($\sim$1380 $\Omega^{-1}\,cm^{-1}$). It is suggested by the authors that this abnormal enhancement is mainly generated by intrinsic contributions, due to the modulated electronic structure by the local disorder effect of the doped atoms, based on theoretical calculations [20]. Therefore, it will be very illuminating to investigate what really happens to the electron band structure of $Co_3Sn_2S_2$ when doped with Ni. Lohani *et al.* have performed angle-resolved photoemission spectroscopy (ARPES) measurements on the significantly doped $Co_{3-x}Ni_xSn_2S_2$ with $x = 0.6$, which reveals the shift of several bands compared to the pristine compound, and the emergence of an extra electron pocket near E_F that is occupied by added electrons [25].

Here, we study the band-structure evolution of $Co_{3-x}Ni_xSn_2S_2$ with $x = 0$, 0.11, and 0.17 at different temperatures by infrared spectroscopy, which is another important technique to explore the band structure near the E_F [26]. We find that the interband transition peak associated with the inverted energy gap near the Weyl points shows a redshift with a small amount of Ni doping, but disappears completely with an excessive amount of Ni doping. This is consistent with the theoretical calculation of the previous report, and possibly responsible for the significant enhancement of the AHE. Our work provides detailed information towards

*These authors contributed equally to this work.
†Contact author: ekliu@iphy.ac.cn
‡Contact author: rychen@bnu.edu.cn

revealing the underlying mechanism of the tuning of AHE by chemical doping.

II. EXPERIMENTAL TECHNIQUES

Three $Co_{3-x}Ni_xSn_2S_2$ single crystals with nominal concentrations of $x = 0$, 0.11, and 0.17 were synthesized by the Sn and Pb mixed flux method [20]. Infrared spectroscopic studies were performed with the Fourier transform infrared spectrometer Bruker 80V in the frequency range from 50 to 40 000 cm^{-1}, on the as-grown shiny surfaces of the three samples. To obtain the absolute value of reflectivity $R(\omega)$, *in situ* gold and aluminum overcoating techniques were employed to eliminate the effect of a microscopic surface texture of the single-crystalline compounds [27]. The real part of the optical conductivity $\sigma_1(\omega)$ is derived from the Kramers-Kronig transformation of the reflectivity $R(\omega)$, which is extrapolated to zero at low frequency by the Hagen-Rubens relation and to high frequency by the x-ray atomic scattering function [28]. Since the experimental data of the reflectivity spectra were measured up to 40 000 cm^{-1}in the ultraviolet region, the high-frequency extrapolation has little influence on the low-frequency behavior of the real part of conductivity via the Kramers-Kronig transformation.

III. RESULTS AND DISCUSSION

The reflectivity $R(\omega)$ and the real part of optical conductivity spectra $\sigma_1(\omega)$ of $Co_{3-x}Ni_xSn_2S_2$ ($x = 0$, 0.11, and 0.17) measured at different temperatures are shown in Fig. 1. As can be seen in the six insets, the overall profiles of the $R(\omega)$ and $\sigma_1(\omega)$ spectra of the three samples are very similar to each other, especially at high energies above 1000 cm^{-1}. This implies that the doping of Ni only modifies the band structure in a very mild way. It is worth mentioning that the spectra of the pristine $Co_3Sn_2S_2$ are consistent with the earlier reports [29,30], which demonstrate the following main characters: (1) At low frequencies, the $R(\omega)$ spectra approach to unit at zero frequency and increase as the temperature decreases, indicative of a metallic response. The $\sigma_1(\omega)$ spectra display associated Drude features around zero energy. (2) Two infrared-active phonon signals show up at 160 and 370 cm^{-1}, respectively. (3) The $R(\omega)$ spectra exhibit a broad absorption structure around 200–300 cm^{-1}, which corresponds to a Lorentz-type peak in the optical conductivity, as denoted by the red arrows in Figs. 1(a) and 1(d). This peak is thoroughly discussed in previous reports and is ascribed to the interband transition across the inverted band gap close to the Weyl nodes around the E_F [29,30]. (4) Two Lorentz-type peaks appear at around 1900 and 5000 cm^{-1}, above which the spectra overlap with each other at different temperatures.

Upon doping, the first two of these characters stays almost unchanged. Particularly, the stability of the phonon frequencies indicates that the lattice structure is quite robust against doping. The most remarkable variation is observed at the low-energy region, as can be seen in the main panels of Fig. 1. The absorption feature in $R(\omega)$ of the pristine compound obviously weakens in $Co_{3-x}Ni_xSn_2S_2$ with $x = 0.11$, and the corresponding Lorentz peak shifts to lower energies, as indicated by the red arrows in the main panels of Figs. 1(b) and 1(e). The weakening and redshifting of this peak indicate the narrowing of the inverted band gap, which agrees well with theoretical calculations [20]. With further doping of $x = 0.17$, the absorption structure in $R(\omega)$ and the associated Lorentz-type peak are completely out of sight, as can be seen in Figs. 1(c) and 1(f). There are two possible explanations for these phenomena: One is that the inverted gap is totally closed, and the other one is that the E_F simply moves out of this gap. We will revisit this issue later and discuss it in more detail.

In order to capture the delicate modification of band structure by doping, we use the Drude-Lorentz model to decompose the optical conductivity $\sigma_1(\omega)$. The dielectric function of the Drude-Lorentz model can be expressed as

$$\varepsilon(\omega) = \varepsilon_\infty - \sum_s \frac{\omega_{ps}^2}{\omega^2 + \frac{i\omega}{\tau_{Ds}}} + \sum_j \frac{S_j^2}{\omega_j^2 - \omega^2 - \frac{i\omega}{\tau_j}},$$

where ε_∞ is the dielectric constant at high energy, the middle term is the Drude component, which describes the electrodynamics of itinerant carriers, and the last term is the Lorentz component that characterizes the excitation of the energy gap or interband transition. The fitting results of $\sigma_1(\omega)$ at 10 and 300 K for all three samples are shown in the main panels and insets of Figs. 2(a)–2(c), respectively. The specific fitting parameters below 3000 cm^{-1} are shown in Table I. It is worth noting that at room temperature the optical conductivity can be well reproduced by one Drude and one Lorentz term below 3000 cm^{-1} for all three samples. By contrast, the spectra become more complicated and more Drude/Lorentz terms are required at low temperatures.

The pristine $Co_3Sn_2S_2$ compound experiences a FM phase transition at $T_C = 175$ K, below which the Drude peak becomes much sharper and extra Lorentz peaks show up in the $\sigma_1(\omega)$ spectra. In previous infrared studies, Yang *et al.* described the emergent feature with one Lorentz peak [29], whereas Xu *et al.* suggested multiple Lorentz peaks [30]. Here, we find our data could be well reproduced by a single Lorentz peak. According to previous reports, this emergent Lorentz peak is ascribed to an interband transition associated with the inverted band gap close to the Weyl nodes, which locates at 339.8(0.5) cm^{-1} at 10 K. As can be seen from Table I, the Ni doping of $x = 0.11$ causes the shift of the emergent Lorentz peak to 270(2) cm^{-1}. This infers that the band gap of the interband transition related to the Weyl nodes is quantitatively reduced. As a result, the integrated Berry curvature is expected to be elevated, and hence leads to the enhancement of the AHE.

With further doping of $x = 0.17$, we find that an additional Drude term is needed to well reproduce the $\sigma_1(\omega)$ at low temperatures, instead of a Lorentz peak as in $Co_3Sn_2S_2$ and $Co_{2.89}Ni_{0.11}Sn_2S_2$. It seems that there is a fundamental change to the band structures caused by the excessive amount of Ni doping. As mentioned earlier, one possible scenario is that the inverted energy gaps near the E_F are fully closed. However, considering that neither the lattice structure nor the FM phase transition are noticeably modified by doping ($T_C = 163$ K when $x = 0.11$, and $T_C = 152$ K when $x = 0.17$ [20]), we believe that the inverted band gap will survive as well, which is guaranteed by the spin-orbital coupling. Therefore, it is more likely that the E_F shifts out of the inverted band gap

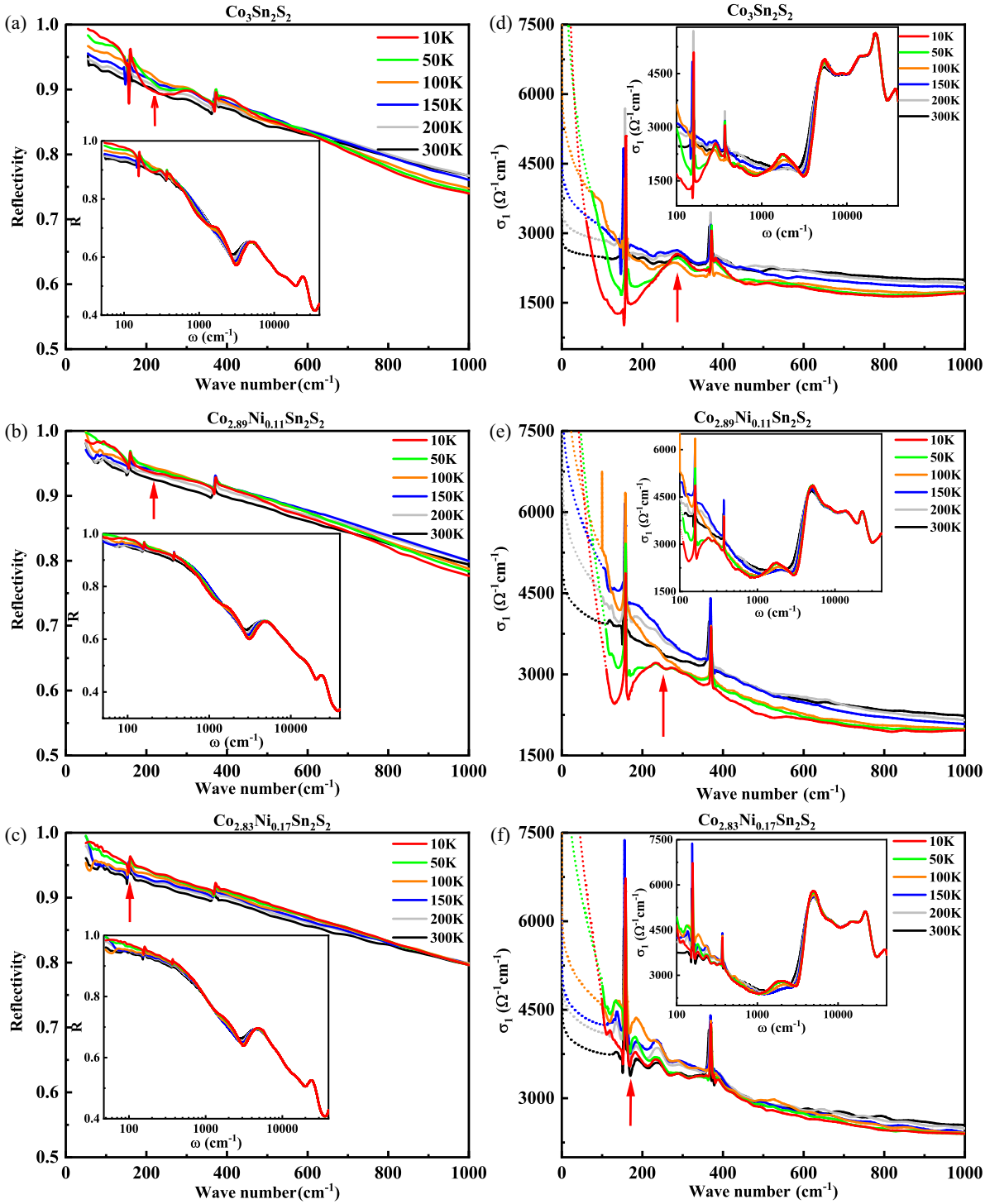

FIG. 1. (a)–(c) Optical reflectivity spectra of $Co_{3-x}Ni_xSn_2S_2$ ($x = 0$, 0.11, and 0.17) single crystals at six different temperatures. The insets show the spectra up to 40 000 cm^{-1}. (d)–(f) The real part of optical conductivity $\sigma_1(\omega)$ of $Co_{3-x}Ni_xSn_2S_2$ obtained through the Kramers-Kronig (KK) transformation. The insets show the expanded $\sigma_1(\omega)$ spectra up to 40 000 cm^{-1}. The extrapolated part through the KK transformation is represented by the dotted line.

and crosses with the initial conduction band. Consequently, some interband transitions disappear from the $\sigma_1(\omega)$ spectra and extra intraband transitions emerge, which agrees perfectly with our results. Moreover, this scenario is also consistent with the theoretical prediction that E_F is pushed upwards upon doping, and the ARPES results where an extra electron pocket appears near E_F, occupied by added electrons. In this case, the AHE is not as large as when the E_F is inside the inverted gap.

The low-energy Drude component represents the response of free carriers, which becomes narrower with temperature decreasing for all three samples, showing good metallicity. In order to extract the doping effect, we plot the optical

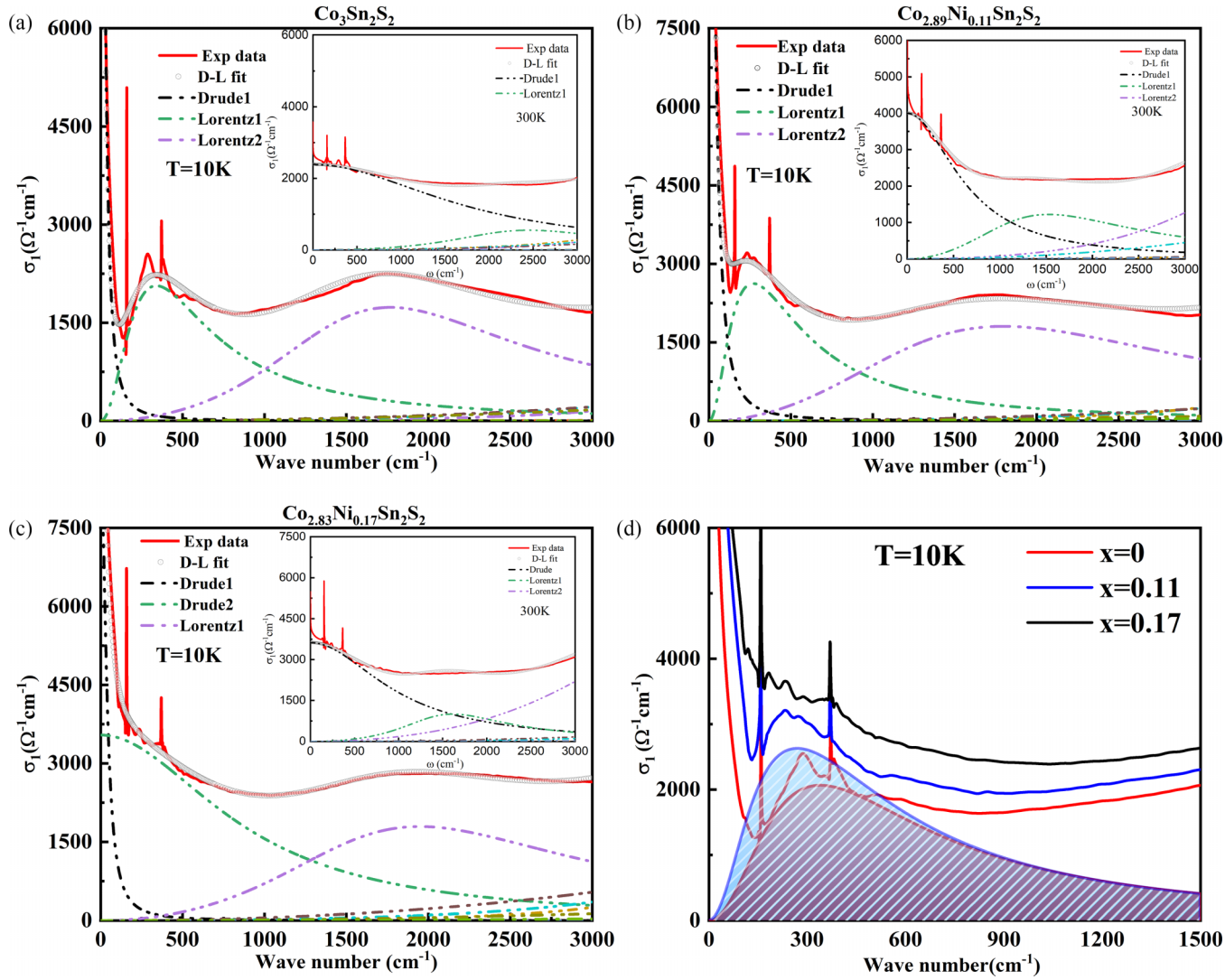

FIG. 2. The Drude-Lorentz fittings of optical conductivity $\sigma_1(\omega)$ at $T = 10$ K for (a) $x = 0$, (b) $x = 0.11$, and (c) $x = 0.17$, while the corresponding Drude-Lorentz fittings of $\sigma_1(\omega)$ at $T = 300$ K are shown in each inset. (d) Experimental real parts $\sigma_1(\omega)$ of the optical conductivity at low energies for three samples at $T = 10$ K. The emergent Lorentz peak features in the $\sigma_1(\omega)$ obtained by Drude-Lorentz fitting are present when $x = 0$ and 0.11, respectively.

conductivity spectra at 10 K in Fig. 2(d). It is clearly seen that the Drude peak broadens with increasing of the doping level. For $Co_3Sn_2S_2$ and $Co_{2.89}Ni_{0.11}Sn_2S_2$, the low-energy part can be well fitted by only one Drude component, whereas two of them are required to fit the low-frequency part of $Co_{2.83}Ni_{0.17}Sn_2S_2$. The two Drude terms represent free carriers from different Fermi surfaces, one of which gradually emerges below T_C. As shown in Table I, the scattering rate of the first Drude component of $Co_{2.83}Ni_{0.17}Sn_2S_2$ [37.6(0.3) cm^{-1}] is actually comparable to that of $Co_3Sn_2S_2$ [24.2(0.1)

TABLE I. The fitting parameters of $\sigma_1(\omega)$ for three samples below 3000 cm^{-1} for 10 and 300 K in the unit of cm^{-1}. ω_p is the plasma frequency and $\gamma_D = 1/\tau$ is the scattering rate of free carriers. ω_j, $\gamma_i = 1/\tau_j$, and S_j represent for the resonance frequency, the width, and the square root of the oscillator strength of Lorentz terms, respectively. The errors of all fitting parameters are included.

x	T (K)	ω_{p1}	γ_{D1}	ω_{p2}	γ_{D2}	ω_1	γ_1	S_1	ω_2	γ_2	S_2
$x = 0$	10	4754(3)	24.2(0.1)			339.8(0.5)	705(3)	9340(10)	1767(1)	1923(6)	14140(30)
	300	16010(20)	1793(6)						2451(4)	2220(20)	8570(50)
$x = 0.11$	10	6040(10)	36.9(0.3)			270(2)	618(9)	9860(70)	1800(20)	2650(80)	16900(300)
	300	12480(40)	650(5)						1530(10)	2170(70)	12600(200)
$x = 0.17$	10	4420(20)	37.6(0.3)	13380(70)	830(10)				1970(20)	2550(90)	16800(500)
	300			14660(80)	990(10)				1610(20)	1500(80)	9500(400)

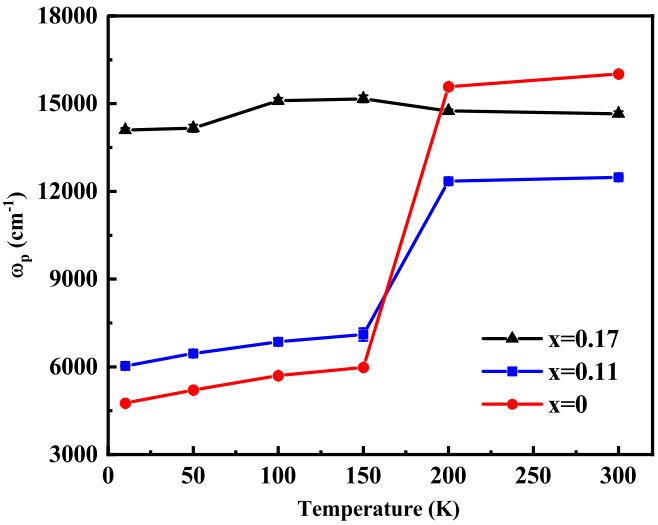

FIG. 3. The temperature-dependent plasma frequency ω_p of $Co_{3-x}Ni_xSn_2S_2$ ($x = 0$, 0.11, and 0.17).

FIG. 4. The real part of optical conductivity $\sigma_1(\omega)$ of $Co_{3-x}Ni_xSn_2S_2$ ($x = 0$, 0.11, and 0.17) at 10 K up to 8000 cm^{-1}. For the sake of clarity, the y axis of $Co_{2.83}Ni_{0.17}Sn_2S_2$ is multiplied by a scale factor of 0.82.

cm^{-1}] and $Co_{2.89}Ni_{0.11}Sn_2S_2$ [36.9(0.3) cm^{-1}], which infers that the disorder effect on the corresponding conduction band is mild. Meanwhile, the scattering rate of the second Drude term of $Co_{2.83}Ni_{0.17}Sn_2S_2$ is much larger, which is absent in $Co_3Sn_2S_2$ and $Co_{2.89}Ni_{0.11}Sn_2S_2$, and hence contributes a large portion of extra itinerant carriers.

The carrier density n can be reflected by the plasma frequency $\omega_p^2 = 4\pi ne^2/m^*$, where m^* is the effective mass of electrons. The overall plasma frequency for two Drude components can be extracted from $\omega_p = (\omega_{p1}^2 + \omega_{p2}^2)^{1/2}$. As shown in Fig. 3, ω_p of the undoped $Co_3Sn_2S_2$ decreases abruptly by entering the FM phase, due to the opening of energy gaps. Although the FM phase transition is barely affected by doping, this sudden decrease of ω_p becomes less obvious in $Co_{2.89}Ni_{0.11}Sn_2S_2$ and totally disappears in $Co_{2.83}Ni_{0.17}Sn_2S_2$, which resembles the evolvement of the emergent Lorentz peak. On the other hand, with the increase of Ni concentration, the total plasma frequency at 10 K is substantially enhanced, especially when $x = 0.17$. Note that the Hall effect measurements of $Co_{3-x}Ni_xSn_2S_2$ demonstrate that the carrier concentration n first decreases monotonically with Ni doping until $x = 0.15$, and then it increases slightly up to $x = 0.17$ [20]. This disagreement between n and ω_p indicates the change of m^* upon doping, which is totally reasonable considering that $Co_{3-x}Ni_xSn_2S_2$ is a Weyl semimetal with nonrelativistic quasiparticles, and there are bands shifting along with doping.

At last, we want to discuss the band-structure modification induced by doping in a wider energy range. To observe the shift of peaks more clearly, we draw the conductivity spectra of three samples at 10 K in a wide frequency range up to 8000 cm^{-1} in Fig. 4, where the spectra are shifted vertically for comparison. For the pristine compound, two prominent peaks at around 1900 and 5000 cm^{-1} could be resolved above 1000 cm^{-1}, which are labeled as Inter1 and Inter2. Inter1 is only noticeable below T_C, and the spectra around the same energies are quite flat at higher temperatures, as shown in Fig. 1(d). Similar behaviors are observed in the doped compounds as well, as can be seen in Figs. 1(e) and 1(f), indicating an identical origination. Compared to the undoped compound, Inter1 is almost unchanged at the doping level of $x = 0.11$ at 10 K, but becomes less sharp at $x = 0.17$. This might be caused by the broadening of the associated valence and conduction bands, which is a natural consequence of the local disorder effect introduced by doping. Remarkably, band broadening is also believed to be responsible for the narrowing of the inverted band gap, which is crucial to the enhancement of the AHE [20]. As for Inter2, the peak position and left side slope are treated as a measurement of electron correlation by former studies [29,30]. Upon doping, we find that although these two parameters are very close to the values of the pristine compound, they differ from sample to sample. Therefore, the change of correlation strength induced by doping remains elusive.

IV. CONCLUSION

In summary, we systematically study the optical spectroscopy of $Co_{3-x}Ni_xSn_2S_2$ crystals at $x = 0$, 0.11, and 0.17. We find that the interband transition peaks associated with the inverted energy gaps close to the Weyl nodes get smaller with Ni doping of $x = 0.11$, but disappear completely with $x = 0.17$. Considering that an extra Drude component shows up in the $x = 0.17$ compound, we deduce that the E_F shifts out of the inverted band gap in this system. These results are consistent with previous theoretical calculations, which are essential to the abnormal enhancement of the AHE. In addition, we also discover that the interband transition peak at around 1900 cm^{-1} is almost unchanged at a doping level of $x = 0.11$ at 10 K, but becomes less sharp at $x = 0.17$, which indicates the broadening of the related conduction and valence bands. This is also believed to be responsible for the narrowing of the inverted band gap, which is crucial to the enhancement of the AHE. Our results not only provide experimental evidence of band-structure modification that is crucial to the enhancement of AHE, but also offer different

insights about the chemical tuning of AHE of topological materials.

ACKNOWLEDGMENTS

This work was supported by the National Key Projects for Research and Development of China (Grants No. 2021YFA1400400 and No. 2022YFA1403800), the National Natural Science Foundation of China (Grant No. 12074042), the Strategic Priority Research Program (B) of the Chinese Academy of Sciences (CAS) (XDB33000000), and the Young Scientists Fund of the National Natural Science Foundation of China (Grant No. 11704033). This work was supported by the Synergetic Extreme Condition User Facility (SECUF).

[1] E. Hall, Philos. Mag. **12**, 157 (1881).
[2] A. Kundt, Ann. Phys. **285**, 257 (1893).
[3] M. V. Berry, Proc. Math. Phys. Eng. Sci. **392**, 45 (1984).
[4] J. Smit, Physica **24**, 39 (1958).
[5] L. Berger, Phys. Rev. B **2**, 4559 (1970).
[6] T. Jungwirth, Q. Niu, and A. H. MacDonald, Phys. Rev. Lett. **88**, 207208 (2002).
[7] M. Onoda and N. Nagaosa, J. Phys. Soc. Jpn. **71**, 19 (2002).
[8] F. D. M. Haldane, Phys. Rev. Lett. **93**, 206602 (2004).
[9] N. Nagaosa, J. Sinova, S. Onoda, A. H. MacDonald, and N. P. Ong, Rev. Mod. Phys. **82**, 1539 (2010).
[10] X. Wang and J. Tan, Appl. Phys. Lett **121**, 161903 (2022).
[11] S. Nakatsuji, N. Kiyohara, and T. Higo, Nature (London) **527**, 212 (2015).
[12] Q. Wang, S. Sun, X. Zhang, F. Pang, and H. Lei, Phys. Rev. B **94**, 075135 (2016).
[13] S. H. Lee, Y. Zhu, Y. Wang, L. Miao, T. Pillsbury, H. Yi, S. Kempinger, J. Hu, C. A. Heikes, P. Quarterman, W. Ratcliff, J. A. Borchers, H. Zhang, X. Ke, D. Graf, N. Alem, C.-Z. Chang, N. Samarth, and Z. Mao, Phys. Rev. Res. **1**, 012011(R) (2019).
[14] A. A. Burkov, M. D. Hook, and L. Balents, Phys. Rev. B **84**, 235126 (2011).
[15] Z. Fang, N. Nagaosa, K. S. Takahashi, A. Asamitsu, R. Mathieu, T. Ogasawara, H. Yamada, M. Kawasaki, Y. Tokura, and K. Terakura, Science **302**, 92 (2003).
[16] A. A. Burkov, Phys. Rev. Lett. **113**, 187202 (2014).
[17] P. V. C. Medeiros, S. Stafström, and J. Björk, Phys. Rev. B **89**, 041407(R) (2014).
[18] E. Liu, Y. Sun, N. Kumar, L. Muechler, A. Sun, L. Jiao, S.-Y. Yang, D. Liu, A. Liang, Q. Xu *et al.*, Nat. Phys. **14**, 1125 (2018).
[19] Q. Wang, Y. Xu, R. Lou, Z. Liu, M. Li, Y. Huang, D. Shen, H. Weng, S. Wang, and H. Lei, Nat. Commun. **9**, 3681 (2018).
[20] J. Shen, Q. Yao, Q. Zeng, H. Sun, X. Xi, G. Wu, W. Wang, B. Shen, Q. Liu, and E. Liu, Phys. Rev. Lett. **125**, 086602 (2020).
[21] J. Shen, Q. Zeng, S. Zhang, H. Sun, Q. Yao, X. Xi, W. Wang, G. Wu, B. Shen, Q. Liu, and E. Liu, Adv. Funct. Mater. **30**, 2000830 (2020).
[22] J. Liu, L. Ding, L. Xu, X. Li, K. Behnia, and Z. Zhu, J. Phys.: Condens. Matter **35**, 375501 (2023).
[23] H. Zhou, G. Chang, G. Wang, X. Gui, X. Xu, J.-X. Yin, Z. Guguchia, S. S. Zhang, T.-R. Chang, H. Lin, W. Xie, M. Z. Hasan, and S. Jia, Phys. Rev. B **101**, 125121 (2020).
[24] G. S. Thakur, P. Vir, S. N. Guin, C. Shekhar, R. Weihrich, Y. Sun, N. Kumar, and C. Felser, Chem. Mater. **32**, 1612 (2020).
[25] H. Lohani, P. Foulquier, P. L. Fèvre, F. Bertran, D. Colson, A. Forget, and V. Brouet, Phys. Rev. B **107**, 245119 (2023).
[26] M. Dressel, G. Gruener, and G. F. Bertsch, Am. J. Phys. **70**, 1269 (2002).
[27] C. C. Homes, M. Reedyk, D. Cradles, and T. Timusk, Appl. Opt. **32**, 2976 (1993).
[28] D. B. Tanner, Phys. Rev. B **91**, 035123 (2015).
[29] R. Yang, T. Zhang, L. Zhou, Y. Dai, Z. Liao, H. Weng, and X. Qiu, Phys. Rev. Lett. **124**, 077403 (2020).
[30] Y. Xu, J. Zhao, C. Yi, Q. Wang, Q. Yin, Y. Wang, X. Hu, L. Wang, E. Liu, G. Xu *et al.*, Nat. Commun. **11**, 3985 (2020).